

PLASMA CONDENSATION IN SOLAR CORONAL LOOPS: II. “CATASTROPHIC COOLING” AND HIGH-SPEED DOWNFLOWS

D.A.N. Müller^{1,2}, H. Peter¹, and V.H. Hansteen²

¹Kiepenheuer-Institut für Sonnenphysik, Schöneckstr. 6, D-79104 Freiburg, Germany, Email:
dmueller@kis.uni-freiburg.de, peter@kis.uni-freiburg.de

²Institute of Theoretical Astrophysics, University of Oslo, P.O. Box 1029, Blindern N-0315, Oslo, Norway, Email:
Viggo.Hansteen@astro.uio.no

ABSTRACT

The second part of this work focuses on the application of the concept of plasma condensation to large coronal loops. In contrast to the short loops analyzed in Müller et al. (2003a), these models can more easily be compared to SOHO and TRACE observations. From our numerical calculations of coronal loops we find several classes of time-dependent solutions (static, periodic, irregular), depending on the spatial dependence of a *temporally constant* energy deposition in the loop. One of these classes is in remarkably close agreement with the features observed with TRACE, described by Schrijver (2001): Emission in C IV (154.8 nm), developing initially near the loop tops, cool plasma sliding down on both sides of the loop, downflow velocities of up to 100 km/s, and a downward acceleration which is substantially reduced with respect to the solar surface gravity. Furthermore, these results also offer an explanation for the observations of De Groof et al. (2003a,b). In contrast to earlier models, we suggest that the process of catastrophic cooling does not have to be initiated by a drastic decrease of the loop heating. It can also result from a loss of equilibrium at the loop apex which is a natural consequence if the loop is heated predominantly at the footpoints, but *constant* in time.

Key words: Sun: corona; Sun: transition region; Sun: UV radiation.

1. INTRODUCTION

Recent observations of the solar transition region and corona, especially with SOHO and TRACE instruments, have shown that closed magnetic structures in the upper solar atmosphere, commonly referred to as coronal loops, exhibit an intrinsically dynamic behavior. Even in quiescent, non-flaring conditions, these loops show strong temporal variability of emission in UV spectral lines and substantial plasma flows. Kjeldseth-Moe & Brekke (1998), e.g., report significant changes of loop systems

over a period of one hour, in particular seen in emission lines in the temperature range between $T = 1 - 5 \cdot 10^5$ K. This variability is accompanied by high Doppler shifts, typically around $v = 50 - 100$ km/s. Recent CDS and EIT observations with high temporal cadence (Fredvik 2002, private communication, De Groof et al., 2003a,b) reveal furthermore spatially localized brightenings in coronal loops, which could be associated with plasma condensations, moving rapidly down towards the footpoints of coronal loops. Schrijver (2001) presents a detailed study of catastrophic cooling and evacuation of quiescent coronal loops observed with the TRACE instrument. He analyzes image sequences taken in different spectral passbands and finds that loop evacuation occurs frequently after plasma in the upper parts of the loops has cooled to transition region or even lower temperatures. The cooling process is often accompanied by emission in Ly α and C IV (154.8 nm), developing initially near the loop tops. Thereafter cool plasma is observed to slide down on both sides of the loops, forming clumps which move with up to 100 km/s. The downward acceleration of these plasma clumps as inferred from these observations is significantly less than the solar surface gravity. The fact that coronal loops can undergo rapid evacuation has been known for decades: Levine & Withbroe (1977), e.g., report *Skylab* spectroscopic observations, compatible with ‘dramatic evacuation’ of active region loops triggered by rapid, radiation dominated cooling. According to the recent observations of Schrijver (2001), this process of dramatic cooling and evacuation is a rather common one. Further observational evidence of ‘blobs’ of plasma falling down towards the solar surface along magnetic field lines is presented by De Groof et al. (2003b). In this paper, we present numerical models of coronal loops which exhibit a wide range of dynamics using a very simple heating function that is exponentially decreasing with height, but constant in time. A key feature of these models is the recurrent formation of plasma condensations, followed by loop evacuation, as described in Müller et al. (2003a,b), which offers a unifying explanation for different aspects of recent observations.

2. NUMERICAL MODEL

In this work, we use the same numerical model as in Müller et al. (2003a,b), and the reader is referred to this work and to Hansteen (1993) for details. Our code solves the one-dimensional time-dependent hydrodynamic equations for mass, momentum and energy conservation, coupled with the ionization rate equations for several elements and self-consistent radiative losses. The plasma is assumed to be effectively thin, and the radiative losses are due to collisional excitation of the various ions comprising the plasma and thermal bremsstrahlung. Thermal conduction, radiative losses and a coronal heating term are included in the energy equation. We include the radiative losses of the elements hydrogen, helium, carbon, oxygen, neon, and iron. While some of the metals are treated by assuming ionization equilibrium and then deriving an *a priori* radiative loss curve as a function of electron temperature, radiative losses from the ions specifically mentioned in this study, i.e. losses from hydrogen, helium, carbon and oxygen, are computed consistently with full time-dependent rate equations.

2.1. Loop Heating and Initial State

We parametrize the energy input into the coronal loop by specifying the energy flux amplitude at the footpoints of the loop, F_{m0} , and assuming a mechanical heat flux that is constant up to a height z_1 and then decreases for $z \geq z_1$ as

$$F_m(z) = F_{m0} \exp[-(z - z_1)/H_m] \quad (1)$$

with a damping length H_m . In the models presented below, we will vary H_m between 2 and 12.5 Mm for a loop of 100 Mm length, while all other parameters have the same values as in Müller et al. (2003a). As an initial state we use the solution of a loop with a large energy dissipation length of $H_m = 12.5$ Mm which has relaxed to a steady state. The resulting loop apex temperature is $T = 7.7 \cdot 10^5$ K.

3. RESULTS

As stated by, e.g., Antiochos et al. (1999), Karpen et al. (2001) and Müller et al. (2003b), for very short damping lengths, solutions with a hot loop apex may no longer exist due to the insufficient energy supply to the center of the loop. In this case, a thermal instability occurs and leads to a run-away cooling process, accompanied by plasma condensation. Unless this condensation region is gravitationally supported by means of, e.g., a dip in the magnetic field lines to maintain a stable prominence-like state, such a configuration with $\nabla \rho \cdot \vec{g} < 0$ is Rayleigh-Taylor unstable. Due to this instability, the condensation region eventually moves down the loop legs and drains through the footpoints. The depleted loop now reheats quickly as its heat capacity is initially very low, and is filled again by chromospheric evaporation. How this cycle of plasma condensation, draining, and chromospheric evaporation is realized exactly depends strongly on the

spatial dependence of the energy deposition. We present here the different types of loop evolution which result from different damping lengths of the heating function. Fig. 1 shows the mean temperature¹, $\langle T \rangle$, of a loop of 100 Mm length as a function of time for damping lengths of $H_m = 2, 3, 5$ and 6 Mm. We find that for large damping lengths ($H_m \geq 6$ Mm), a stable, static solution is attained with a mean temperature of $\langle T \rangle \approx 5 \cdot 10^5$ K. For shorter damping lengths, the loop shows a periodic variation of $\langle T \rangle$ due to the cycle of condensation – draining – evaporation discussed above. For even shorter damping lengths ($H_m \leq 2.5$ Mm), the evolution of $\langle T \rangle$ is irregular and shows intermittency of hot phases and strongly fluctuating cool phases. This type of intermittent behavior is well-known from chaotic non-linear systems.

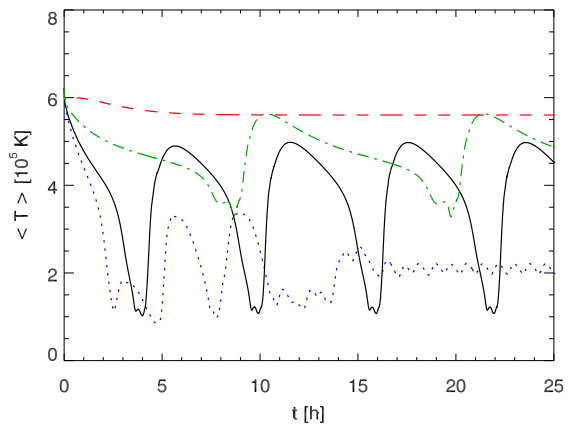


Figure 1. Evolution of mean temperature, $\langle T \rangle$, as a function of time, for different damping lengths of the heating function: $H_m = 2$ Mm (dotted), $H_m = 3$ Mm (solid), $H_m = 5$ Mm (dash-dotted), $H_m = 6$ Mm (dashed).

These different classes of solutions can also be visualized in a $\langle T \rangle$ – $\langle p \rangle$ diagram (Fig. 2): In this diagram, fixed points correspond to static solutions ($H_m = 6$ Mm), limit cycles correspond to periodic solutions ($H_m = 3, 5$ Mm), and irregular orbits correspond to irregular solutions. It should be noted that these diagrams do not represent a phase-space but simple establish a relation between the mean values of different physical variables which characterize this system.

Having introduced the general characteristics of the system, let us now examine the different types of dynamic solutions in more detail. In Fig. 3 we plot space-time diagrams of the loop temperature, $T(z, t)$, for $H_m = 5, 3, 2$ Mm. Due to space limitations only parts of the whole time series obtained from the model calculations are displayed.

In the first case ($H_m = 5$ Mm, *left* plot), one condensation region forms at a given time at the loop apex and

¹The mean values are defined as the average quantities over the region of the loop which lies above the transition region, bounded by the points where the temperature crosses $T = 10^5$ K in both loop legs (the exact choice of this cutoff value does not significantly influence the results).

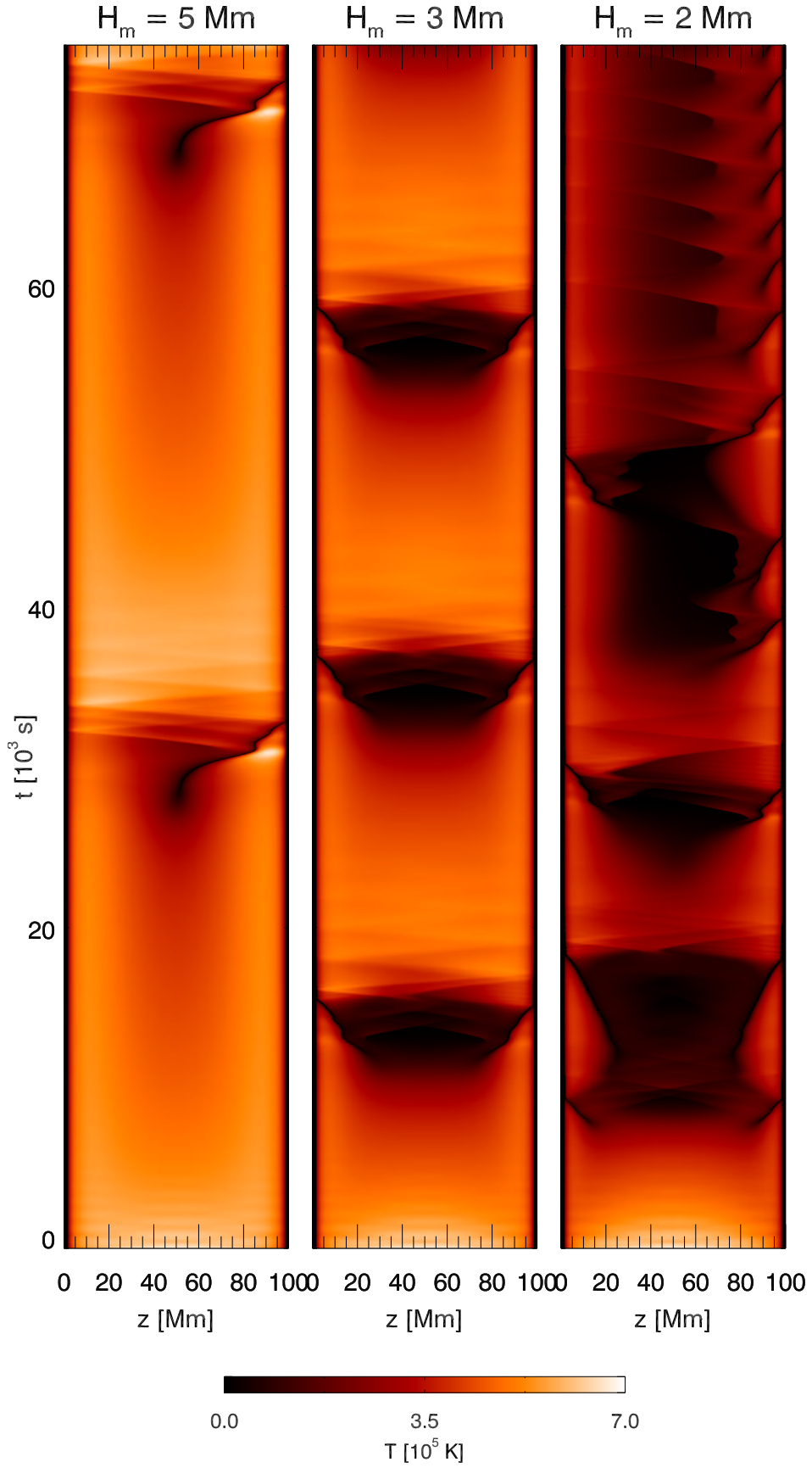


Figure 3. Evolution of temperature for three different damping lengths of the heating function: $H_m = 5 \text{ Mm}$ (left), $H_m = 3 \text{ Mm}$ (center), $H_m = 2 \text{ Mm}$ (right).

the plasma is then accelerated to velocities of ≈ 100 km/s on its way down (the highest velocities are found in the wake of the condensation region). When this condensation region encounters the transition region, it is strongly decelerated by the pressure gradient of the underlying plasma and the velocity profile forms a shock wave (cf. Sect. 5). As the compression is approximately adiabatic, this leads to a transient heating of the transition region plasma. The *center* plot of Fig. 2 ($H_m = 3$ Mm) shows the second type of recurrent condensations which occurs if the damping length is slightly reduced with respect to the first case. Here, two condensation regions form simultaneously and then drain down both loop legs. In both cases, i.e. $H_m = 5$ Mm and $H_m = 3$ Mm, the loop temperature exhibits a periodic variation with time. The third panel of Fig. 3 ($H_m = 2$ Mm) shows the most interesting evolution of this set of numerical experiments: As the heating is now even more concentrated towards the footpoints, the evolution of temperature along the loop with time reflects the persistent battle between loop heating and radiative cooling which results in an irregular sequence of plasma condensation, draining and reheating, accompanied by strong flows and transient brightenings of transition region lines.

4. SPECTRAL SIGNATURE OF CATASTROPHIC COOLING AND DOWNFLOWS

As our numerical code consistently solves the atomic rate equations for different atomic species, we can calculate the non-equilibrium emission of a large number of coronal spectral lines. In this context, the emission lines of C IV (154.8 nm) (formation temperature $T_f \approx 10^5$ K) and O V (63.0 nm) ($T_f \approx 2.2 \cdot 10^5$ K) are of particular interest since the 155 nm passband filter of TRACE is dominated by C IV emission (at least above the limb), and the O V line is frequently observed with SOHO/CDS. Fig. 4 shows a cutout from Fig. 3 (*center*), together with a velocity map. In Fig. 5 space-time diagrams of the corresponding emission in the two spectral lines are plotted. It is seen that the condensation regions are accompanied by strong brightenings in both C IV and O V.

5. FORMATION OF A SHOCK WAVE

In a hydrostatic configuration, the gravitational force acting on the plasma is balanced by the pressure gradient. As an illustration of a temporarily static phase of the dynamic loop model with $H_m = 3$ Mm, we plot in Fig. 6 (*upper left panel*) the component of the gravitational acceleration parallel to the loop, $g_{\parallel}(z)$, and the acceleration due to the pressure gradient, $\nabla p(z)/\rho(z)$, along the coronal part of the loop for $t = 32000$ s. It is seen that these two quantities compensate each other, and due to this equilibrium, the plasma in the loop is nearly static (the velocity is displayed in the *upper right panel*). At $t = 34400$ s, however, a loss of equilibrium has occurred and the gravitational force is no longer balanced by the pressure gradient (*lower left panel*): In the central part of the loop, the pressure gradient has dropped to

very small values, while close to the footpoints, it is more than an order of magnitude higher than the gravitational acceleration. This explains the velocity profile seen in the *lower right panel*: In the central part of the loop, the plasma is accelerated to velocities very close to the free-fall speed, indicated by the *dashed* line, and then strongly decelerated in the lower parts of the loop, resulting in a characteristic shock profile.

6. SUMMARY

Our model calculations of coronal loops offer an explanation for observations of catastrophic cooling and high-speed downflows, using a very simple, time-independent heating function. The non-linearity of the energy equation results in a loss of equilibrium which triggers a highly dynamic loop evolution. No external time-dependent driving mechanism is necessary to explain rapid cooling and evacuation of loops. Coronal loops can exhibit cyclic behavior, with a wide range of periods, as well as irregular evolution. A first, qualitative comparison with observational data (De Groof et al., 2003a,b) looks promising, and we will extend our model to loops comparable to the ones observed and carry out a detailed analysis. A further investigation of the model results presented here is in preparation.

REFERENCES

- Antiochos, S. K., MacNeice, P. J., Spicer, D. S., & Klimchuk, J. A. 1999, ApJ, 512, 985
- De Groof, A., Berghmans, D., Van Driel-Gesztelyi, L., & Poedts, S. 2003a, in Proceedings of the SOHO-15 workshop, ed. H. Lacoste (ESA SP-547), these proceedings
- De Groof, A., Berghmans, D., Van Driel-Gesztelyi, L., & Poedts, S. 2003b, A&A, in press
- Hansteen, V. 1993, ApJ, 402, 741
- Karpen, J. T., Antiochos, S. K., Hohensee, M., Klimchuk, J. A., & MacNeice, P. J. 2001, ApJ, 553, L85
- Levine, R. H. & Withbroe, G. L. 1977, Sol. Phys., 51, 83
- Müller, D. A. N., Hansteen, V., & Peter, H. 2003a, in Proceedings of the SOHO-15 workshop, ed. H. Lacoste (ESA SP-547), these proceedings
- Müller, D. A. N., Hansteen, V., & Peter, H. 2003b, A&A, in press
- Schrijver, C. J. 2001, Sol. Phys., 198, 325

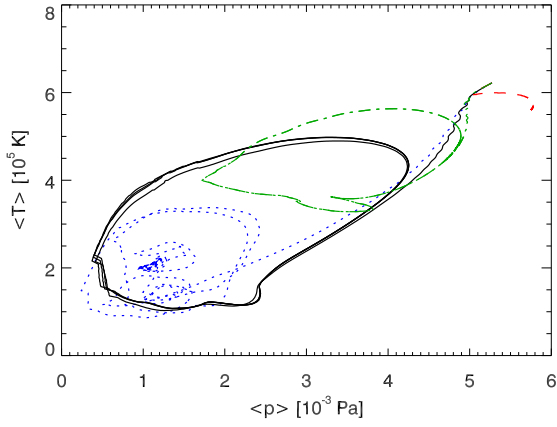


Figure 2. $\langle T \rangle$ ($\langle p \rangle$) diagram for different damping lengths of the heating function: $H_m = 2$ Mm (dotted), $H_m = 3$ Mm (solid), $H_m = 5$ Mm (dash-dotted), $H_m = 6$ Mm (dashed).

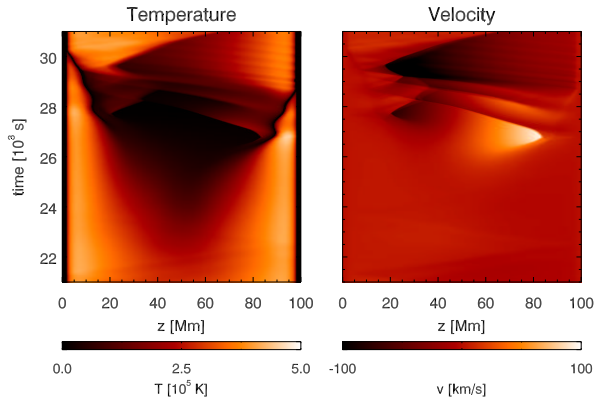


Figure 4. Formation of two condensation regions in a coronal loop. The left plot shows the evolution of temperature along the loop, the right plot shows the corresponding velocities. The region shown here is a cutout from Fig. 3, right panel.

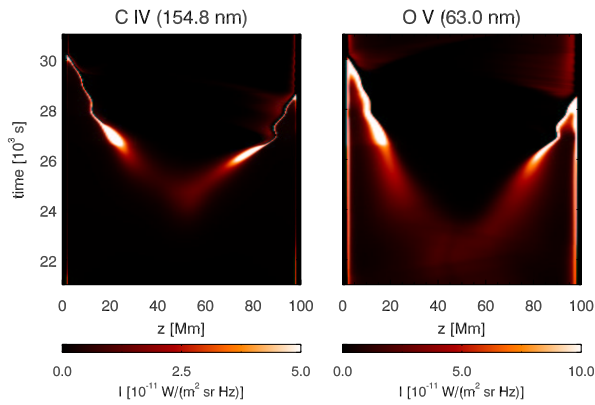


Figure 5. Transient brightenings accompanying the condensation regions. Left: Emission in C IV (154.8 nm), right: emission in O V (63.0 nm.)

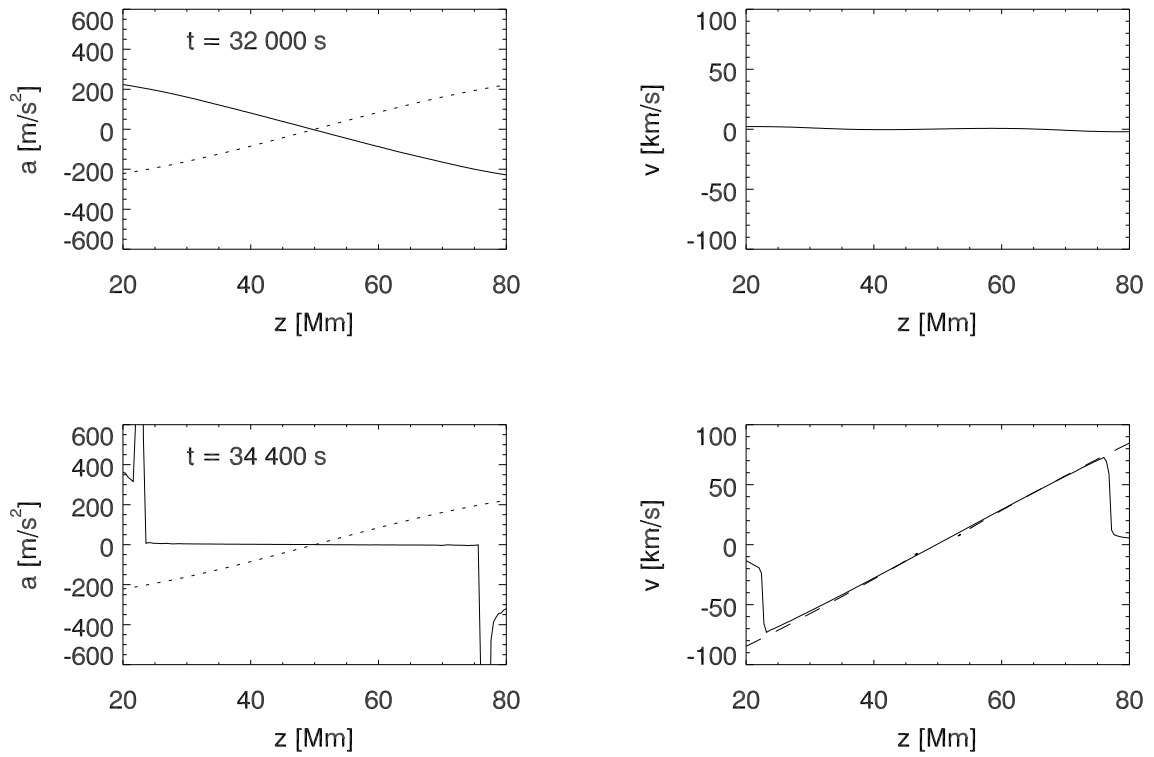


Figure 6. Formation of a shock wave for $H_m = 3 \text{ Mm}$. Gravitational acceleration, $g_{\parallel}(z)$ (dashed), and acceleration due to the pressure gradient, $\nabla p(z)/\rho(z)$ (solid), for $t = 32\,000 \text{ s}$ (top row) and $t = 34\,400 \text{ s}$ (bottom row). In the lower right plot, the free-fall velocity profile is indicated by a dashed line.